





# Assessing space and time changes in daily maximum temperature in the Ebro basin (Spain) using model-based statistical tools

Ana C. Cebrián<sup>1</sup>  | Jesús Asín<sup>1</sup>  | Jorge Castillo-Mateo<sup>1</sup>  |  
Alan E. Gelfand<sup>2</sup>  | Jesús Abaurrea<sup>1</sup>

<sup>1</sup>Department of Statistical Methods,  
University of Zaragoza, Zaragoza, Spain

<sup>2</sup>Department of Statistical Science, Duke  
University, Durham, North Carolina, USA

## Correspondence

Ana C. Cebrián, Department of Statistical  
Methods, University of Zaragoza, Pedro  
Cerbuna 12, Zaragoza 50009, Spain.  
Email: [acebrian@unizar.es](mailto:acebrian@unizar.es)

## Funding information

MCIN/AEI/10.13039/501100011033,  
Grant/Award Numbers:  
TED2021-130702B-I00,  
PID2020-116873GB-I00; Unión Europea  
NextGenerationEU; Gobierno de Aragón

## Abstract

There is continuing interest in the investigation of change in temperature over space and time. For this analysis, we offer statistical tools to illuminate changes temporally, at desired temporal resolution, and spatially, using data generated from suitable space–time models. The proposed tools can be used with the output from any suitable model fitted to any set of spatially referenced time series data. The tools to assess space and time changes include spatial surfaces of probabilities and spatial extents for events defined by exceeding a threshold. The spatial surfaces capture the spatial variation in the probability or risk of an exceedance event, while the spatial extents capture the expected proportion of incidence of an event for a region of interest. This approach is used to analyse the changes in daily maximum temperature in an inland Mediterranean region (NE of Spain) in the period 1956–2015. The area is very heterogeneous in orography and climate, including the central Ebro valley and part of the Pyrenees. We use a collection of daily temperature series obtained from simulation under a Bayesian daily temperature model fitted to 18 stations in that area. The results for the summer period show that, although there is an increasing risk in all the events used to quantify the effects of climate change, it is not spatially homogeneous, with the largest increase arising in the centre of the Ebro valley and the Eastern Pyrenees area. The risk of an increase in the average daily maximum temperature from 1966–1975 to 2006–2015 higher than 1°C is higher than 0.5 over all of the region, and close to 1 in the previous areas. The extent of daily maximum temperature higher than the reference mean has increased 3.5% per decade. The mean of the extent indicates that 95% of the area under study has suffered a positive increment of the average temperature, and almost 70% an increment higher than 1°C.

## KEYWORDS

Bayesian temperature model, climate risk map, space–time analysis, spatial extent, surface of probabilities

This is an open access article under the terms of the [Creative Commons Attribution-NonCommercial](https://creativecommons.org/licenses/by-nc/4.0/) License, which permits use, distribution and reproduction in any medium, provided the original work is properly cited and is not used for commercial purposes.

© 2023 The Authors. *International Journal of Climatology* published by John Wiley & Sons Ltd on behalf of Royal Meteorological Society.

## 1 | INTRODUCTION

Climate change is a global phenomenon, and the interest in assessing global warming in a spatiotemporal framework is clear. Studies to assess and quantify the trends and effects of climate change on temperature usually focus on the study of spatially aggregated signals or on the individual study of local time series (Gil Alana & Sauci, 2019). However, individual study is limiting, because it does not allow us to assess the nature of changes that may occur over a spatial region of interest. Further, studying spatially aggregated data sacrifices insight into local variation in behaviour. Concerning the time scale, many spatial analyses model annual or seasonal summaries of temperature, see Masson-Delmotte et al. (2021) for a review. However, the use of a daily scale is important, since it allows us to incorporate the inherent variability of data while still enabling aggregation to a desired broader time scale. This scale is also essential to study persistence of temperatures. In addition, many environmental applications require temperature data at this scale.

The contribution of this work is the analysis in a space–time framework of the changes in daily maximum temperature in an inland Mediterranean region around Aragón (NE of Spain) in the period 1956–2015. The study of this area is relevant because an increasing trend in the mean temperature is detected on Spanish mainland (Peña-Angulo et al., 2021). Further, the region includes heterogeneous areas showing relevant climate variability. The heterogeneity arises from the arid central valley of the Ebro basin to mountain areas, such as the southern slopes of the Pyrenees where a large part of the region's water resources are located. This type of analysis is challenging since assessment of space and time changes in daily maximum temperature using empirical approaches has many limitations, particularly the inability to assess uncertainty. Dowlatabadi and Morgan (1993) noted that uncertainty consideration should be an integral part of the integrated assessment of climate change. Also, Katz (2002) strongly advised the use of full-fledged uncertainty analysis as part of climate assessment, recommending probabilistic modelling and, in particular, Bayesian hierarchical modelling and Markov chain Monte Carlo (MCMC) simulation techniques. By now many space–time environmental science models have been proposed in a Bayesian framework (Craigmile & Guttorp, 2011; Crimp et al., 2015).

In this framework, we offer a set of statistical tools to analyse space–time changes on the evolution of daily maximum temperatures in a region using data generated from Bayesian space–time models, or any

suitable model-based stochastic weather generator (SWG). Suitable SWGs are those that enable simultaneous generation of series for arbitrary unobserved sites (Caraway et al., 2014; Smith et al., 2018; Wilks, 1999, 2009). More precisely, the required data is a collection (replicates) of daily temperature series at a fine grid of geo-coded locations in the region under study. Some SWGs providing this type of data are based on Bayesian models (see, e.g., Kleiber et al., 2013 or Verdin et al., 2019).

In this work, the space–time analysis in the study area is carried out using a collection of posterior predictive gridded daily maximum temperature series obtained from the Bayesian model developed in Castillo-Mateo et al. (2022). This model was fitted using observed daily maximum temperatures at  $n=18$  sites, from 1956 to 2015. It is a rich autoregressive mean model which captures needed spatial dependence through four Gaussian processes (GPs) modelling intercepts, slope/trend coefficients, variances and autocorrelations, respectively. While alternative models could be proposed, the model we employ was validated for this dataset in Castillo-Mateo et al. (2022) to reproduce the statistical properties of the central part of the daily temperature distribution.

We offer two main strategies for quantifying the effect of climate change on different features of temperature, each with associated uncertainty. The first calculates probabilities that will be useful in climate risk assessment. According to Katz (2002), the quantification of uncertainty in the form of probabilities is required as input to any decision or risk analysis. The United Nations Framework Convention on Climate Change (UNFCCC) defines climate risk as the probability of exceeding one or more criteria of vulnerability. The approach suggested in this work aims to compute the occurrence probabilities of this type of event, defined by exceeding a threshold. Further, this procedure enables calculation of maps of surface of probabilities for the events of interest, capturing the spatial behaviour of the probability of a given excess over threshold event.

The second strategy formalizes the concept of an extent to investigate a useful objective in spatial climate analysis, that is, to characterize the extent of occurrence of a specific feature within a given area. More precisely, the extent associated with a given region reflects the proportion of the region in which the event is expected to occur. We can specify this at daily scale but further, we can average over days to attach this inference to coarser time scales. Using this approach, we are able not only to identify the areas where a feature of interest occurs but also to quantify the mean and uncertainty of the percentage of area where that feature occurs. There are previous studies

analysing the idea of extent of extreme temperatures using observed data (Keellings & Moradkhani, 2020; Rebetez et al., 2009) or climate model output (Khan et al., 2019; Lyon et al., 2019). However, they employed descriptive approaches precluding formal inference. Some formal concepts related to the notion of an extent have been introduced in the statistical literature. Bolin and Lindgren (2015) and Sommerfeld et al. (2018) consider excursion sets, which are sets of points in an area where a spatial function is above a given threshold. Haug et al. (2020) identified excursion sets in Europe with significant trends in summer mean temperature. Cebrián et al. (2022) defined the notion of the extent of an extreme heat event as a stochastic object and used it to calculate daily, seasonal and decadal averages. Excursion sets and level sets are examples of local events whose proportion of incidence, that is, prevalence over a subregion of interest, enables greater insight into temperature behaviour.

In the presented analysis, we consider events having a temperature higher than the corresponding local mean, or an increase in the mean temperature between two decades higher than a given value. In addition, any other event defined in terms of the available time series and a specified threshold can be considered. Using the proposed strategies, we compute the probabilities of a positive increment of temperature between two decades. Further, we characterize, for a given day within a given year, what proportion of the subregion was above a choice of a local reference temperature during 1 day or during a run of consecutive days, in order to study persistent temperatures. Moreover, we study the behaviour of these extents over time and also comparatively between subregions. Since our generating model is autoregressive, correlation structure in the series is captured and we can formally investigate persistence. More precisely, we can study runs of days within the same climate event, which is a common approach to study this feature (Pfleiderer & Coumou, 2018; Tye et al., 2019). These persistent events are particular cases of the compound events defined by Zscheischler et al. (2020). The importance of the study of the effects of climate change on temperature persistence is underscored by Li and Thompson (2021).

The paper is structured as follows. Section 2 describes the observed temperature series and the space–time model by Castillo-Mateo et al. (2022) used to generate the grid of replicates of temperature series. Section 3 presents the proposed tools and the different events considered in the space–time analysis. Section 4 summarizes the results of the analysis of two types of events, those based on the comparison of temperature with a reference value, and those based on the temperature increments between two decades. It also shows the comparison of the evolution of the extent in two areas with different climates. Finally,

section 5 summarizes the main conclusions and future work. Data S1, Supporting Information contains additional exploratory analyses and further results.

## 2 | REGIONAL SETTING AND MODEL TO GENERATE DATA

The regional setting and the dataset are presented in section 2.1 and the model fitted to it in section 2.2.

### 2.1 | Regional setting and exploratory analysis

The study area is located in the Ebro basin (85,362 km<sup>2</sup>), in the northeast of Spain (see Figure 1). Different climate subareas can be distinguished, due to its location in the Iberian Peninsula and its heterogeneous orography that includes the Ebro valley (centre) where elevations descend to 200 m, and mountains: Pyrenees (north), Cantabrian Range (northwest) and Iberian System (southwest). The mountains reach 3000 m in the Pyrenees and 2000 m in the Iberian System. Mediterranean-continental dry climate with irregular rainfall and a large temperature range is the prevailing climate, but also mountain climates are present in the region. This variety of climate conditions is one reason for interest in the area.

Figure 1 shows the location of the 18 sites where daily maximum temperature observed series, from 1956 to 2015, are available. They have been provided by the Spanish Meteorological Office (AEMET). Temperature in this region shows seasonal behaviour, with large differences between winter and summer months; for example, in Zaragoza (the main city in the region) this difference is around 22°C. This seasonal pattern is quite spatially homogeneous in the area.

Castillo-Mateo et al. (2022) performed a thorough exploratory analysis of the the daily maximum temperatures for the three summer months, JJA, over these 18 sites, and a summary of this analysis is shown in sect. S1 of Data S1. According to this exploratory analysis, spatial variability in the mean temperatures is linked to elevation, where Panticosa is the highest and coldest location and La Puebla de Híjar in the valley is the hottest. However, elevation is not sufficient to explain the mean temperature variability, since there are areas at the south and north of the Ebro river, with similar elevation, around 1000 m, and different mean temperatures. The standard deviations of the series show the maximum variability is in the northwest, 5.6°C in Pamplona, and the minimum in the southwest, 4.1°C in Cueva Foradada. The serial correlation is over 0.90 for all series, reflecting temperature inertia in the short term. It is a key

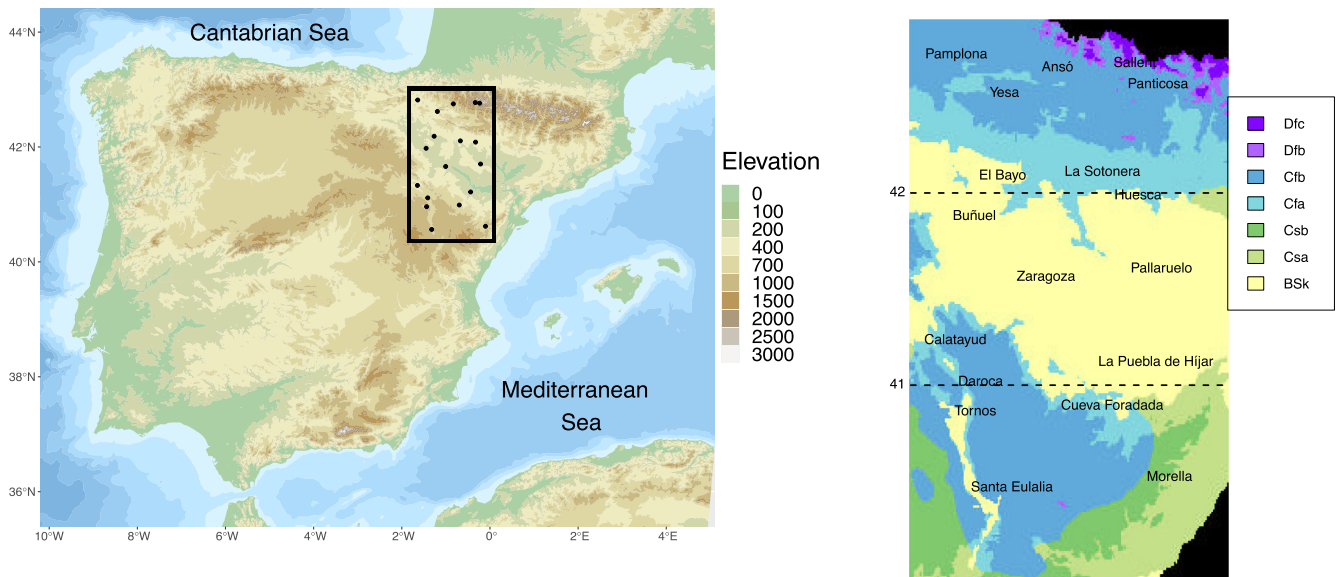


**FIGURE 1** (left) Relief map of the region under study and location of observed temperature series. (right) Climate classification of the region (Chazarra-Bernabé et al., 2018) [Colour figure can be viewed at [wileyonlinelibrary.com](https://onlinelibrary.wiley.com/doi/10.1002/joc.8305)]

distributional feature to be considered in presenting the statistical inference. To explore the observed change over time, linear trends are estimated in each series using the observations in the period JJA 1956–2015. Spatially heterogeneous behaviour is found in this feature, with the smallest changes in the western observatories and the largest in the valley.

With regard to spatial dependence, a strong correlation is observed between daily temperature series in different sites, and therefore, it should be incorporated into the analysis. Pairwise Pearson coefficients between the series at two sites are calculated separately for each month to avoid the correlation caused by the common seasonal pattern. The 25th percentile of all pairwise coefficients is 0.82 in June, 0.74 in July and 0.73 in August.

Finally, to explore changes over time and space, we consider the “empirical extent” for the event defined as the increment of daily maximum temperature above a reference mean  $\tilde{\mu}(\mathbf{s})$  higher than a value  $c$ . The empirical extent is computed as the observed proportion of the 18 available stations where the event occurs. Figure 2 summarizes the average of the empirical extent over days in JJA of each year during the period 1966–2015 for events based on increments over the reference mean  $\tilde{\mu}(\mathbf{s})$  higher than  $c = 0, 1$  and  $2^\circ\text{C}$ . Here,  $\tilde{\mu}(\mathbf{s})$  is a reference mean (the mean for JJA in 1966–2015) that is site-specific but constant over time. The fitted linear trend shows an increase of the empirical extent of 0.037 per decade for increases over  $\tilde{\mu}(\mathbf{s})$  higher than 0 and 0.041 for increases higher than  $2^\circ\text{C}$ . An evident limitation of this empirical extent is that it is based on only 18 stations.

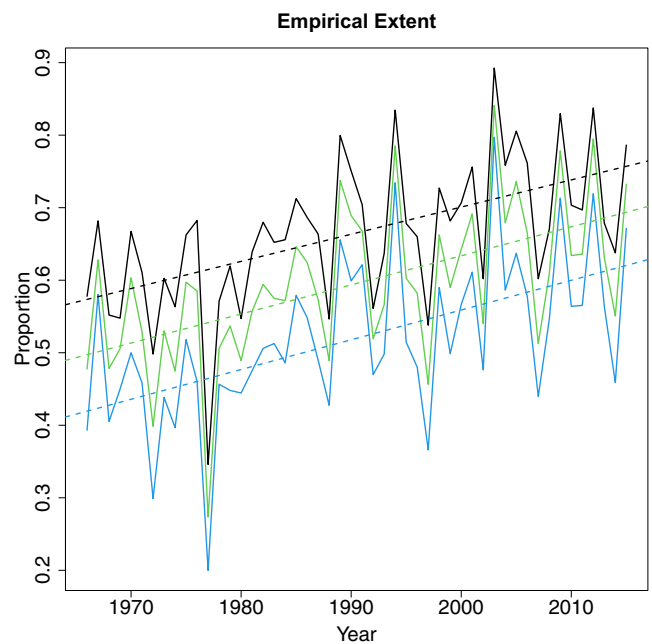


**FIGURE 2** Yearly averages in JJA of the empirical extent, calculated with the 18 stations, for increments over the reference mean  $\tilde{\mu}(\mathbf{s})$  higher than 0 (black),  $1^\circ\text{C}$  (green) and  $2^\circ\text{C}$  (blue) and linear trends fitted over time [Colour figure can be viewed at [wileyonlinelibrary.com](https://onlinelibrary.wiley.com/doi/10.1002/joc.8305)]

## 2.2 | A space–time model to generate daily maximum temperatures

The tools suggested in this work will be used to analyse the temperature evolution in Aragón using as input the posterior realizations of daily temperature obtained from



the spatiotemporal model in Castillo-Mateo et al. (2022). This is a complex model fitted in a Bayesian framework but, as noted above, any alternative model able to generate adequate replicates of time series at a fine grid of geocoded locations could be used equally well to generate the temperature realizations required; for example, the space–time model by Schliep et al. (2021) or the SWG by Verdin et al. (2019).

A brief summary of this model is included in this section, but all the fitting and validation details and a thorough motivation of the model can be found in Castillo-Mateo et al. (2022). It is noteworthy that the model in Castillo-Mateo et al. (2022) was fitted using observations from the warm period from May to September. Here, we will only consider the series for JJA, even though the model can generate series for all 5 months. An exploratory analysis of the temperature dataset showed that a statistical model for daily temperatures must include terms that capture the seasonal behaviour, the spatially heterogeneous standard deviation and trend, as well as the temporal and spatial dependence observed in the region. To obtain the desired behaviour, we introduce both fixed effects terms, that capture elevation as well as trend and seasonal patterns, and random effects terms that capture spatial and temporal dependence. Then, the daily maximum temperature for day  $\ell$  within year  $t$  and location  $\mathbf{s}$ ,  $Y_{t,\ell}(\mathbf{s})$ , is modelled as

$$\begin{aligned} Y_{t,\ell}(\mathbf{s}) &= m_{t,\ell}(\mathbf{s}) + \rho(\mathbf{s})(Y_{t,\ell-1}(\mathbf{s}) - m_{t,\ell-1}(\mathbf{s})) + \varepsilon_{t,\ell}(\mathbf{s}), \\ m_{t,\ell}(\mathbf{s}) &= \mu_{t,\ell}(\mathbf{s}) + \gamma_t(\mathbf{s}), \\ \mu_{t,\ell}(\mathbf{s}) &= \beta_0 + \alpha t + \beta_1 \sin(2\pi\ell/365) + \beta_2 \cos(2\pi\ell/365) + \beta_3 \text{elev}(\mathbf{s}), \\ \gamma_t(\mathbf{s}) &= \beta_0(\mathbf{s}) + \alpha(\mathbf{s})t + \psi_t + \eta_t(\mathbf{s}). \end{aligned} \quad (1)$$

Note that the model introduces temporal dependence using a first-order autoregressive structure on the temperature anomalies, as suggested in the Fifth IPCC Report (Hartmann et al., 2013), with the coefficient  $\rho(\mathbf{s})$  capturing dependence for consecutive days at location  $\mathbf{s}$ . Zwiers and Von Storch (1995) and Chandler and Scott (2011) also state that modelling of the temporal dependence in the data is important since its omission may lead to an inappropriate statistical assessment of the trend. The conditional mean of  $Y_{t,\ell}(\mathbf{s})$  given yesterday's temperature  $Y_{t,\ell-1}(\mathbf{s})$  is expressed by  $m_{t,\ell}(\mathbf{s}) + \rho(\mathbf{s})(Y_{t,\ell-1}(\mathbf{s}) - m_{t,\ell-1}(\mathbf{s}))$ . The model assumes that spatial and temporal dependence is captured by the conditional mean, so that  $\varepsilon_{t,\ell}(\mathbf{s})$  are pure error terms with independent  $N(0, \sigma^2(\mathbf{s}))$  distribution where  $\sigma^2(\mathbf{s})$  is a spatially varying variance.

Here,  $m_{t,\ell}(\mathbf{s})$  contains fixed and random effects,  $\mu_{t,\ell}(\mathbf{s})$  and  $\gamma_t(\mathbf{s})$ , respectively. The daily fixed effects are captured by  $\beta_0$ , a global intercept,  $\alpha t$ , a baseline long-term linear trend,  $\beta_1$  and  $\beta_2$ , the coefficients of a harmonic that captures the seasonal component, and  $\beta_3$ , the coefficient for the elevation at  $\mathbf{s}$ ,  $\text{elev}(\mathbf{s})$ . The annual random effects given in  $\gamma_t(\mathbf{s})$  capture space–time dependence through GP; for details on GPs see, for example, chap 3 in Banerjee et al. (2014). A local spatial adjustment to the intercept,  $\beta_0(\mathbf{s})$ , and a local slope adjustment,  $\alpha(\mathbf{s})$ , enable a flexible, spatially varying, local linear trend. This locally linear trend substantially extends the usual linear trend specification adopted in climate analysis (Masson-Delmotte et al., 2021). The terms  $\psi_t \sim \text{IIDN}(0, \sigma_\psi^2)$  provide annual intercepts to allow for yearly shifts (associated, e.g., with the ENSO), and  $\eta_t(\mathbf{s}) \sim \text{IIDN}(0, \sigma_\eta^2)$  provides local annual intercepts to allow for local yearly shifts.

The model is fitted in a Bayesian framework using MCMC; see Banerjee et al. (2014) and Gelfand and Smith (1990) for details on these methods and sect. S2 of Data S1 for information regarding prior specification.

As a last comment, the result of the Bayesian model fitting is to produce the posterior distribution of any unknown in the model, that is, the conditional distribution of the unknown given the data. Using MCMC to fit the model, we obtain as many samples as we wish from this posterior distribution. From these samples, we can learn arbitrarily well about any features of the distribution of the unknown including say, the mean and variance, as well as interval estimates. That means, that the previous model enables kriging, and it can be used to generate samples of the value of the daily temperature at unobserved locations in the region under study for a given day  $\ell$  within year  $t$ .

## 2.2.1 | Dataset generated from the model

As noted above, a collection of independent replicates, of daily temperature within a year on a spatial grid over  $\mathcal{D}$  for the period of interest,  $\{Y_{t,\ell}^{(b)}(\mathbf{s}) : b=1, \dots, B\}$ , are generated using the model in Equation (1). Note that  $B$  can be as large as we wish; it has no connection to the size of the dataset used to fit the model. As a sample from a predictive distribution, these replicates provide the fundamental material for all of the inference using the tools in the sequel. They will not only allow us to learn about the distribution of temperature at any location on any day but also about the distribution of any other measures of interest that can be computed as functions of temperatures  $Y_{t,\ell}(\mathbf{s})$ , as we describe in the following sections.

We emphasize again that this approach can be implemented using datasets from other generating models. That is, for other datasets, over different regions and appropriate time scales, fitted with different appropriate models, we can follow the same path for enhanced learning about temperature behaviour over space and time.

### 3 | METHODS: NOVEL TOOLS FOR ENRICHING SPACE-TIME ANALYSIS OF EXCESS OVER THRESHOLD EVENTS

We present tools to illuminate the spatial and temporal behaviour of daily maximum temperature. Again, the set  $\{Y_{t,\ell}^{(b)}(\mathbf{s}) : b=1, \dots, B\}$  provides samples of any function of daily temperature over days ( $\ell$ ), years ( $t$ ) or locations ( $\mathbf{s}$ ). Hence, we can “see” the distribution of this function and any features of this distribution that are of interest such as its location, variability or tail behaviour.

A primary intent is to study changes in temperature over time, to quantify their magnitude, and to identify areas with different evolution. To obtain conclusions over space, we use surfaces of probabilities (of risk) and the concept of extent (proportion of area) linked to “events” that allow the quantification of the increase in temperature. The underlying idea is to define events of interest  $A_{t,\ell}(\mathbf{s})$  in terms of the daily maximum temperatures  $Y_{t,\ell}(\mathbf{s})$  and using an excess over threshold approach, for example, the event of maximum temperature at day ( $t, \ell$ ) at location  $\mathbf{s}$  being higher than a site-specific reference value  $r(\mathbf{s})$ ,  $A_{t,\ell}(\mathbf{s}) = \{Y_{t,\ell}(\mathbf{s}) > r(\mathbf{s})\}$ . From a model-generated replicate  $Y_{t,\ell}^{(b)}(\mathbf{s})$ , we can obtain a realization of the binary/indicator variable,  $\mathbf{1}(Y_{t,\ell}(\mathbf{s}) > r(\mathbf{s}))$ , a variable that is equal to 1 if  $Y_{t,\ell}(\mathbf{s}) > r(\mathbf{s})$ , and 0 otherwise. For illustration, all the measures and tools in this section are defined for the simple event  $\{Y_{t,\ell}(\mathbf{s}) > r(\mathbf{s})\}$ . However, they can be applied to any other event defined in terms of  $Y_{t,\ell}(\mathbf{s})$ ; examples of these events are described later in section 3.3. All of the ensuing inference is posterior, that is, conditional given the data. To simplify notation, we suppress the conditioning below, then  $P(A_{t,\ell}(\mathbf{s})|\text{data})$  will be denoted  $P(A_{t,\ell}(\mathbf{s}))$ .

#### 3.1 | Surfaces of probabilities

The posterior probability associated with an event at location  $\mathbf{s}$ ,  $A_{t,\ell}(\mathbf{s})$ , is obtained by calculating the proportion of events in the collection of realizations  $Y_{t,\ell}^{(b)}(\mathbf{s})$ ,

$b=1, \dots, B$ , that is, the mean of the binary variables indicating the occurrence of the event,

$$\widehat{P}(A_{t,\ell}(\mathbf{s})) = \frac{1}{B} \sum_{b=1}^B \mathbf{1}(A_{t,\ell}^{(b)}(\mathbf{s})), \quad (2)$$

where  $A_{t,\ell}^{(b)}(\mathbf{s})$  is the event defined in terms of the  $b$ th realization  $Y_{t,\ell}^{(b)}(\mathbf{s})$ ; for example,  $\{Y_{t,\ell}^{(b)}(\mathbf{s}) > r(\mathbf{s})\}$ .

Events based on daily maximum temperature, such as  $\{Y_{t,\ell}(\mathbf{s}) > r(\mathbf{s})\}$ , are defined for each day ( $t, \ell$ ), so that it is straightforward to summarize them over a period of time. The previous daily probabilities can be summarized by averaging them in a given period, for example, below, the 920 (10×92) days in JJA in a decade  $D$ , denoted by D-JJA,

$$\bar{P}(A(\mathbf{s})) = \frac{1}{920} \sum_{t \in D, \ell \in \text{JJA}} \widehat{P}(A_{t,\ell}(\mathbf{s})). \quad (3)$$

These daily or average probabilities over the grid of points  $\mathbf{s}$  can be plotted and smoothed in a map, to reveal a surface of probabilities, or averaged over a region.

#### 3.2 | Extent for an event

The extent for an event in a region  $\mathcal{B} \subseteq \mathcal{D}$  is defined as the proportion/fraction of incidence of that event in the region (Cebrián et al., 2022). Formally, the extent in  $\mathcal{B}$  for an event  $A_{t,\ell}(\mathbf{s})$  is the stochastic integral,

$$\text{Ext}(A_{t,\ell}(\mathcal{B})) = \frac{1}{\|\mathcal{B}\|} \int_{\mathcal{B}} \mathbf{1}(A_{t,\ell}(\mathbf{s})) d\mathbf{s},$$

where  $\|\mathcal{B}\|$  denotes the area of  $\mathcal{B}$ . Although this integral cannot be calculated explicitly, it can be approximated arbitrarily well by Monte Carlo integration as

$$\widetilde{\text{Ext}}(A_{t,\ell}(\mathcal{B})) = \sum_{\mathbf{s} \in \mathcal{B}} w_{\mathbf{s}} \mathbf{1}(A_{t,\ell}(\mathbf{s})), \quad (4)$$

where  $w_{\mathbf{s}}$  weights the size of the grid cell linked to  $\mathbf{s}$ , which cover region  $\mathcal{B}$ :  $w_{\mathbf{s}} = w_{\mathbf{s}}^* / \sum_{\mathbf{s} \in \mathcal{B}} w_{\mathbf{s}}^*$  for given size grid cell  $w_{\mathbf{s}}^*$ . In other words, it is the weighted average over the region of the binary variables for events  $A_{t,\ell}(\mathbf{s})$ .

We can obtain a realization of an extent from each set of realizations  $Y_{t,\ell}^{(b)}(\mathbf{s})$  for  $\mathbf{s} \in \mathcal{B}$ , and with  $B$  observations of the extent, we obtain its posterior predictive distribution, which is employed for inference. To keep the

notation simple, if the considered region is the entire region,  $\mathcal{B}=\mathcal{D}$ , the argument  $\mathcal{B}$  is omitted.

When we compute daily extents, again, it may be of interest to summarize them by averaging them over a period of time, for example, D-JJA,

$$\overline{\text{Ext}}(A(\mathcal{B})) = \frac{1}{920} \sum_{t \in D, \ell \in \text{JJA}} \widetilde{\text{Ext}}(A_{t,\ell}(\mathcal{B})). \quad (5)$$

Note that the  $B$  realizations available of this average extent will characterize the distribution of the average, not a daily extent. This means that the variance will be much smaller than in the previous example since it is averaged over a large number of terms.

### 3.3 | Defining events to quantify the increase in temperature

There are many ways to define events that allow us to quantify an increase in temperature. Here, we propose several ways to define those events, but any other option that can be evaluated from the daily temperature observations  $Y_{t,\ell}(\mathbf{s})$  can be studied by applying the tools described in the previous section. We consider two general choices of events, one based on increments over a reference value and the other on increments between two periods of time.

First, we consider events defined in terms of the increment in temperature with respect to a reference value  $r(\mathbf{s})$ , which is site-specific but constant across time. The simplest events,  $\{Y_{t,\ell}(\mathbf{s}) - r(\mathbf{s}) > c\}$ , are based on daily maximum temperature; note that these events correspond to events defined as daily temperature higher than a value  $r(\mathbf{s}) + c$ . An important feature of temperature is its persistence across days, so that we define events based on the daily temperature for  $k=2$  or 3 consecutive days  $\{Y_{t,\ell}(\mathbf{s}) - r(\mathbf{s}) > c; 2\} \equiv \{Y_{t,\ell}(\mathbf{s}) - r(\mathbf{s}), Y_{t,\ell+1}(\mathbf{s}) - r(\mathbf{s}) > c\}$  or  $\{Y_{t,\ell}(\mathbf{s}) - r(\mathbf{s}) > c; 3\} \equiv \{Y_{t,\ell-1}(\mathbf{s}) - r(\mathbf{s}), Y_{t,\ell}(\mathbf{s}) - r(\mathbf{s}), Y_{t,\ell+1}(\mathbf{s}) - r(\mathbf{s}) > c\}$ .

An extension is to define events based on an average temperature in a period of time, for example, the average in D-JJA,

$$\bar{Y}_D(\mathbf{s}) = \frac{1}{920} \sum_{t \in D, \ell \in \text{JJA}} Y_{t,\ell}(\mathbf{s}).$$

Then, we define events based on the increment of the average temperature over the reference value,  $\{\bar{Y}_D(\mathbf{s}) - r(\mathbf{s}) > c\}$ .

Another important feature to quantify global warming is the increment of temperature between two periods

of time; here, we will consider the increment between two decades 1966–1975 ( $D1$ ) and 2006–2015 ( $D5$ ). As above, the increments can be defined using daily temperatures or average temperatures. Here we show the analysis of the increment of average temperatures, that is the events  $\{\bar{Y}_{D5}(\mathbf{s}) - \bar{Y}_{D1}(\mathbf{s}) > c\}$ . The analysis of the increments between two decades at a daily scale is presented in sect. S4.1 of Data S1. For clarity, Table 1 summarizes the type and notation of all the events analysed in the following section.

## 4 | RESULTS FOR THE SPACE-TIME ANALYSIS

We apply the methodology described in section 3 to study the effect of climate change on different features related to daily maximum temperature in a Mediterranean area, a region in the Ebro basin. Section 4.1 shows the results over the entire region while a comparison of the extent for different increments of temperatures in two areas with different climates regimes is carried out in section 4.2.

The tools are applied to a set of  $B=500$  replicates of daily maximum temperature  $\{Y_{t,\ell}^{(b)}(\mathbf{s}); b=1, \dots, 500\}$  generated from the model in section 2.2, on a spatial grid covering the area  $\mathcal{D}$  drawn in Figure 1, for the 92 days in JJA in the period 1956–2015. Given the different orography in the study region, a grid with 4401 points  $\mathbf{s}$  with a locally adapted spatial resolution is adopted. The spatial changes in temperature in flat areas are slow so a  $4 \times 4 \text{ km}^2$  grid is used, while in an area in the Pyrenees with a steep relief, the scale of the grid is resolved to

TABLE 1 Events defined to quantify the effects of climate change

| Event                                                         | Definition                                                                                                              |
|---------------------------------------------------------------|-------------------------------------------------------------------------------------------------------------------------|
| $\{Y_{t,\ell}(\mathbf{s}) - r(\mathbf{s}) > c\}$              | Increment of daily maximum temperature over a reference value $r(\mathbf{s})$ , higher than $c$                         |
| $\{Y_{t,\ell}(\mathbf{s}) - r(\mathbf{s}) > c; k\}$           | Increment of daily maximum temperature over a reference value $r(\mathbf{s})$ , higher than $c$ in $k$ consecutive days |
| $\{\bar{Y}_D(\mathbf{s}) - r(\mathbf{s}) > c\}$               | Increment of average temperature in decade $D$ over a reference value $r(\mathbf{s})$ higher than $c$                   |
| $\{\bar{Y}_{D5}(\mathbf{s}) - \bar{Y}_{D1}(\mathbf{s}) > c\}$ | Increment of average temperatures between two decades higher than $c$                                                   |

Note: In this work, events are defined for three values  $c = 0, 1$  and  $2^\circ\text{C}$  and two persistence periods  $k=2$  and 3 days, and the reference value  $r(\mathbf{s})$  is a local mean.

$1 \times 1 \text{ km}^2$ . The first decade of the generated realizations, 1956–1965, is reserved to obtain reference values and the analysis over time is done over the period 1966–2015.

As a simple example of the information provided by the output series, Figure 3 (left) shows, spatially, the difference between the medians in decades  $D1$  and  $D5$  (the medians in each decade are shown in Figure S2). Although the increase is higher than  $0.5^\circ\text{C}$  in all of the region, the map reflects the spatial variability of the area: the highest increases, greater than  $2^\circ\text{C}$  occur in the centre of the valley and the east area of the Pyrenees, while the lowest occur in the NW.

To define the first choice of events, we need a reference value  $r(\mathbf{s})$ . Here, we consider a mean value, but other options, for example a high percentile, could be used to study the evolution of extreme events, provided that the considered data generator from the associated model is able to reproduce adequately the tails of data distribution. Our site-specific reference value  $r(\mathbf{s})$  is the mean temperature in JJA during the reference decade 1956–1965, denoted as the reference mean  $\tilde{\mu}(\mathbf{s})$ . The resulting mean surface is shown in Figure 3 (right); the image is built using the function *pimage* from the R package *autoimage* (French, 2017), that interpolates the previous points on a regular grid using multilevel B-splines. The warmest area, with mean temperature higher than  $30^\circ\text{C}$  is the Ebro river valley, especially the areas closest to the river and the eastern part of the valley, while the coolest areas correspond to the Pyrenees, with mean temperatures lower than  $20^\circ\text{C}$ . We will analyse events for three different increments  $c=0, 1$  and  $2^\circ\text{C}$ . The values

1 and 2 are approximately  $1/4$  and  $1/2$  of the standard deviation of daily maximum temperature, and values in this range are commonly used to evaluate effects of climate warming (IPCC, 2018).

## 4.1 | Analysis of the entire region

### 4.1.1 | Analysis of increments of daily maximum temperature over $\tilde{\mu}(\mathbf{s})$

This section summarizes the results of the analysis of events based on increments of daily maximum temperature over the reference mean,  $\tilde{\mu}(\mathbf{s})$ , for 1 day and persistent events for  $k=2$  and 3 days.

#### Surface of probabilities

The daily posterior probabilities of the previous events are computed using Equation (2), and averaged over D-JJA using Equation (3). Figure 4 shows the averages for decades  $D1$  and  $D5$  of the probabilities of exceeding the reference mean,  $\{Y_{t,c}(\mathbf{s}) - \tilde{\mu}(\mathbf{s}) > 0\}$ . In  $D1$ , the averaged probabilities vary from 0.42 to 0.47. However, clear evidence of global warming is observed in  $D5$ , since the probabilities all over the region are higher, attaining values close to 0.7 in the SW (the area from Zaragoza, next to the Ebro river, to Daroca and Cueva Foradada, with a higher elevation) and also in the NE (Pyrenees area that contains Sallent and Panticosa, the locations with highest elevation in the observed dataset). That means that, in those areas, the reference mean corresponds to the 30th percentile of the temperature

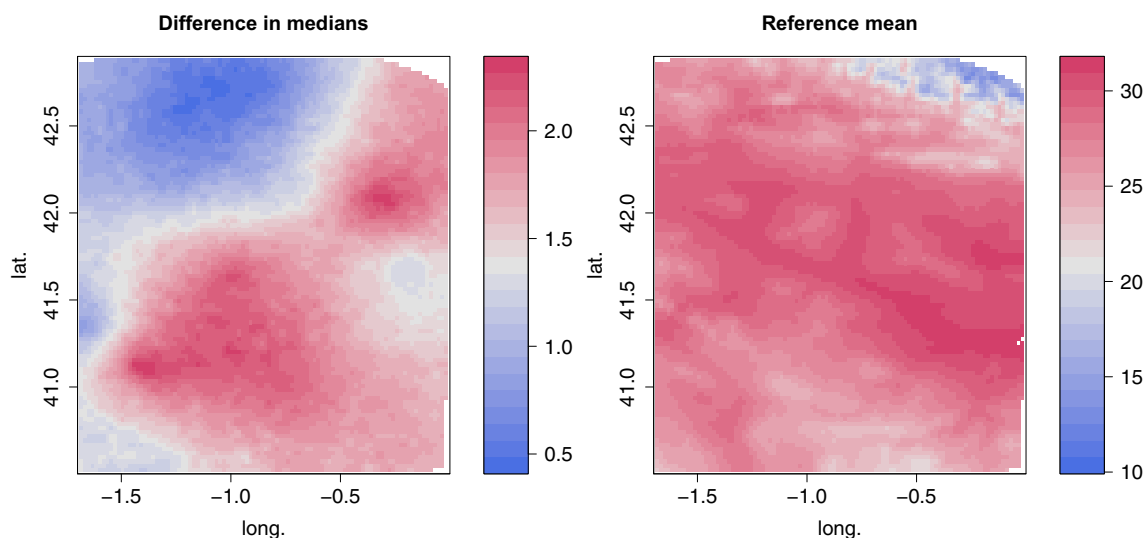


FIGURE 3 (left) Difference in the medians of the daily maximum temperatures ( $^\circ\text{C}$ ) in JJA in decades  $D5$  and  $D1$ . (right) Map of the reference mean  $\tilde{\mu}(\mathbf{s})$ , that is, mean daily temperature ( $^\circ\text{C}$ ) in JJA in the decade 1956–1965 [Colour figure can be viewed at [wileyonlinelibrary.com](https://onlinelibrary.wiley.com)]



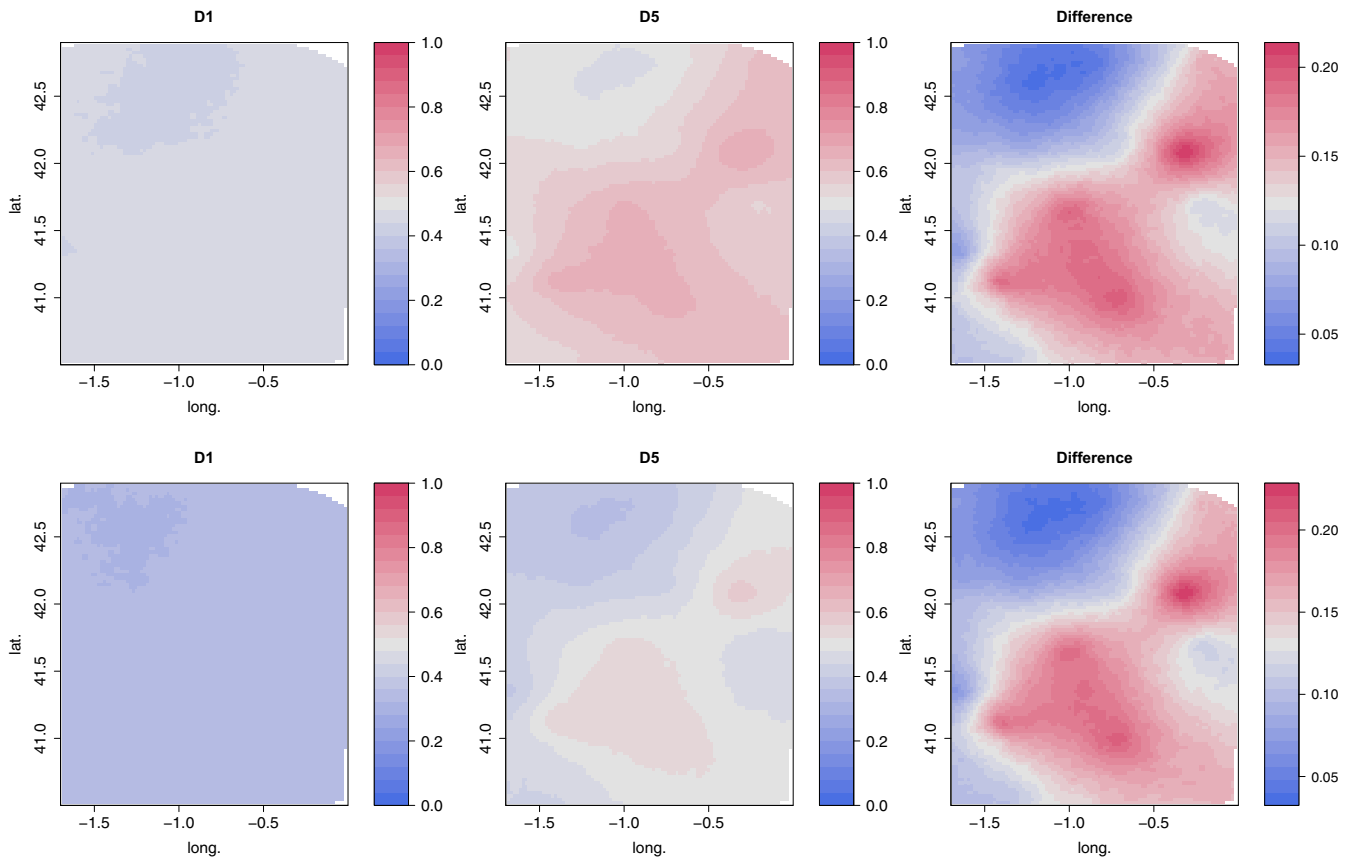


FIGURE 4 Average in D-JJA of probabilities of events  $\{Y_{t,\ell}(\mathbf{s}) - \tilde{\mu}(\mathbf{s}) > 0\}$  (first row) and  $\{Y_{t,\ell}(\mathbf{s}) - \tilde{\mu}(\mathbf{s}) > 2\}$  (second row) in D1 and D5, and difference between them [Colour figure can be viewed at [wileyonlinelibrary.com](http://wileyonlinelibrary.com)]

distribution during D5. There is also evidence of changes in temperature persistence, since the analysis of the events  $\{Y_{t,\ell}(\mathbf{s}) - \tilde{\mu}(\mathbf{s}) > 2\}$  shows that the risk of positive increments over the reference mean during two consecutive days is around 0.3 in D1, and in D5 it varies from the same value 0.3 in the NW, to 0.6.

### Extents

Here, Equation (4) is used to compute extents over the entire region associated with the foregoing events. The average extent for events based on daily temperature are computed employing different periods of time. First, we compute yearly averages  $\overline{\text{Ext}}(A_t(\mathcal{B})) = \frac{1}{92} \sum_{\ell \in \text{JJA}} \widetilde{\text{Ext}}(A_{t,\ell}(\mathcal{B}))$  to study the evolution across years of the events  $A_{t,\ell}(\mathbf{s}) = \{Y_{t,\ell}(\mathbf{s}) - \tilde{\mu}(\mathbf{s}) > 0\}$ . Figure 5 (black line) shows the posterior means of those yearly averages, revealing a roughly linear increase with a trend equal to 0.0035 and 90% credible interval (CI) (0.0030, 0.0039); this means an increase in extent per decade equal to 3.5%. A similar evolution across years is expected in the extent for events defined with different increments and persistence; for example, the linear trends for events with increments higher than  $c = 1$  and  $2^\circ\text{C}$  are equal to 0.0035 and 0.0033, respectively. As an aside, the trend of empirical extents, that is, the proportion of observed stations exceeding

their reference value, shown in Figure 2, is similar, 0.0037, for temperatures over the reference mean. However, an evident limitation of this empirical extent is that uncertainty of the empirical extents cannot be quantified. Moreover, it is defined relative to only 18 stations as opposed to the fine grid of 4401 locations employed in our posterior predictive simulation.

Regarding the average extents over decades  $\overline{\text{Ext}}(A(\mathcal{B}))$ , see Equation (5), Table 2 summarizes their means for events  $\{Y_{t,\ell}(\mathbf{s}) - \tilde{\mu}(\mathbf{s}) > c\}$  with  $c = 0, 1$  and  $2^\circ\text{C}$  in D1 and D5, and for the persistent events defined with 2 and 3 consecutive days. The variability of the average extents is quite low, with 90% CI of length around 0.06 in all the cases. This variability is much lower than the variability across decades, indicating a clear increase in the extent for all types of events; for example, the mean and the 90% CI of the average extent for daily temperatures over  $\tilde{\mu}(\mathbf{s})$  in D1 and D5 are, respectively, 0.45 (0.42, 0.48) and 0.58 (0.55, 0.61). That increase yields a similar extent for events  $\{Y_{t,\ell}(\mathbf{s}) - \tilde{\mu}(\mathbf{s}) > 0\}$  in D1 and the extent for events  $\{Y_{t,\ell}(\mathbf{s}) - \tilde{\mu}(\mathbf{s}) > 2\}$  in D5, that is, 0.41 (0.38, 0.45). As a consequence of this warming, the average extent in D5 with  $c = 1^\circ\text{C}$  is higher than the average in D1 with  $c = 0^\circ\text{C}$ . The increase is also observed in the extent for persistent events based on 3 days, especially in

**TABLE 2** Posterior mean of the average extent in D-JJA for increments of daily maximum temperature over the reference mean, for different values  $c$  and persistence in decades  $D1$  (1966–1975) and  $D5$  (2006–2015); last row shows the mean of the extents for increments of average temperature

| $c$                                                           | 0°C  |      | 1°C  |      | 2°C  |      |
|---------------------------------------------------------------|------|------|------|------|------|------|
|                                                               | $D1$ | $D5$ | $D1$ | $D5$ | $D1$ | $D5$ |
| $\{Y_{t,\ell}(\mathbf{s}) - \tilde{\mu}(\mathbf{s}) > c\}$    | 0.45 | 0.58 | 0.37 | 0.50 | 0.29 | 0.41 |
| $\{Y_{t,\ell}(\mathbf{s}) - \tilde{\mu}(\mathbf{s}) > c; 2\}$ | 0.34 | 0.47 | 0.26 | 0.38 | 0.19 | 0.30 |
| $\{Y_{t,\ell}(\mathbf{s}) - \tilde{\mu}(\mathbf{s}) > c; 3\}$ | 0.26 | 0.39 | 0.19 | 0.31 | 0.13 | 0.23 |
| $\{\bar{Y}_D(\mathbf{s}) - \tilde{\mu}(\mathbf{s}) > c\}$     | 0.26 | 0.78 | 0.05 | 0.47 | 0.01 | 0.17 |

increments higher than  $c = 2^\circ\text{C}$ , where the mean of the average extent in  $D5$  shows a relative increase with respect to  $D1$ , higher than 75%, from 0.13 to 0.23.

#### 4.1.2 | Analysis of increments of average temperature over $\tilde{\mu}(\mathbf{s})$

This section summarizes the analysis of events based on the average temperature in D-JJA,  $\{\bar{Y}_D(\mathbf{s}) - \tilde{\mu}(\mathbf{s}) > c\}$  for decades  $D1$  and  $D5$  and values  $c = 0, 1$  and  $2^\circ\text{C}$ .

##### Surface of probabilities

In  $D1$ , the risk of average temperature higher than  $\tilde{\mu}(\mathbf{s})$  varies slightly throughout the region, from 0.03 to 0.4. In  $D5$ , this risk is much higher (from 0.7 to virtually 1) in all the region except in the NW, the area closer to the Cantabrian Sea (see Figure 6). The pattern of the increase in the risk of this event is different from most of the other events where the areas with highest risk of suffering the effects of climate change are the centre of the valley and the NE areas. Regarding the risk of increments of the average temperature over  $\tilde{\mu}(\mathbf{s})$  being higher than  $1^\circ\text{C}$ , in  $D1$ , it is quite homogeneous throughout the region: lower than 0.08 in 75% of the region and always lower than 0.2. However, although the risk in  $D5$  has increased all over the region, there are relevant differences depending on the area: it varies from values lower than 0.2 in the NW up to more than 0.7 in the central part of the valley.

##### Extents

First, to characterize the evolution over time, we compute the extent of positive increments of the average temperature in JJA in each year  $\{Y_t(\mathbf{s}) - \tilde{\mu}(\mathbf{s}) > 0\}$ . Figure 7 shows the boxplots of the posterior distribution of those yearly extents. The increasing trend of the extent is clear, demonstrating that the variability between years is higher than the variability within year. The slope of these extents is 0.0088, more than double the slope of the extents based on daily temperatures. In addition to the

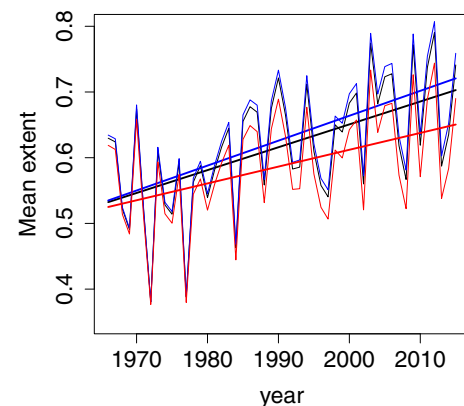


**FIGURE 5** Posterior density of the extent for events  $\{\bar{Y}_D - \tilde{\mu}(\mathbf{s}) > c\}$  with  $c=0$  (solid line) and  $c=1$  (dotted line) in  $D1$  (red) and  $D5$  (blue) [Colour figure can be viewed at [wileyonlinelibrary.com](http://wileyonlinelibrary.com)]

increasing trend, this plot permits us to identify years which were colder with respect to the trend, and with a lower variability, for example, 1972, 1977, 1984, or hotter as year 2003 (García-Valero et al., 2015). In the last decade, two different types of behaviours are observed, the distribution of the extent in some years is quite high, centred around 0.9, while others centred around 0.5.

We also analyse the extent for increments of decadal averages  $\{\bar{Y}_D(\mathbf{s}) - \tilde{\mu}(\mathbf{s}) > c\}$ ; the last row in Table 2 summarizes the posterior mean of those extents with  $c=0, 1$  and  $2^\circ\text{C}$  and Figure 8 compares their posterior densities in  $D1$  and  $D5$  for  $c=0$  and 1. The ratio of the mean extents in  $D5$  and  $D1$  increases with  $c$ : it is equal to 3 for  $c=0$ , 9.4 for  $c=1$ , and 17 for  $c=2^\circ\text{C}$ . The variability of the posterior distribution of these extents is not large so that the probability of the extent for events  $\{\bar{Y}_D(\mathbf{s}) - \tilde{\mu}(\mathbf{s}) > 0\}$  being higher in  $D5$  than in  $D1$  is virtually 1 for the three  $c$  values. A consequence of this increase is that the mean of the extent for increments higher than 0 in  $D1$  is roughly one third its counterpart in  $D5$ , and almost half the extent of increments higher than  $1^\circ\text{C}$  in  $D5$ .

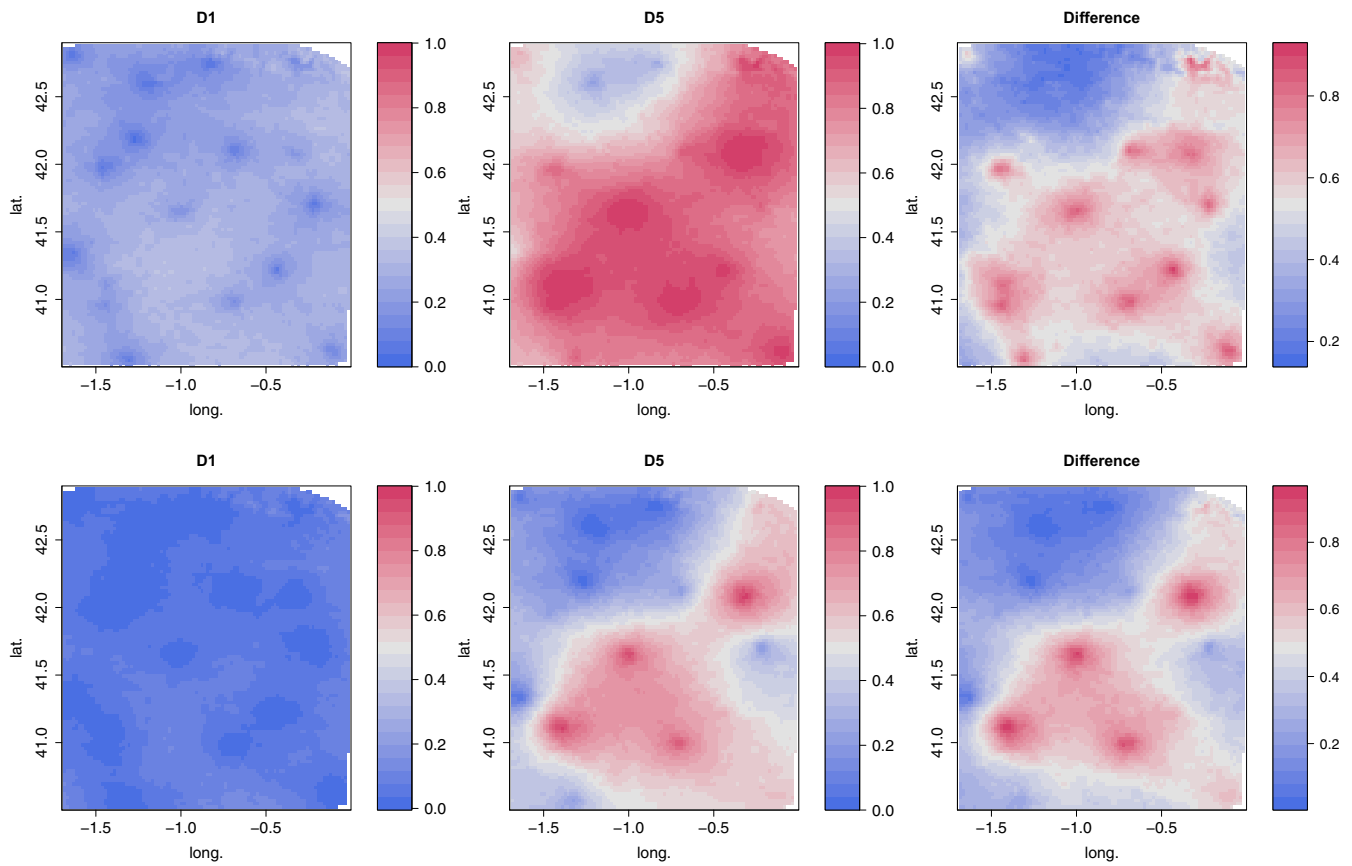
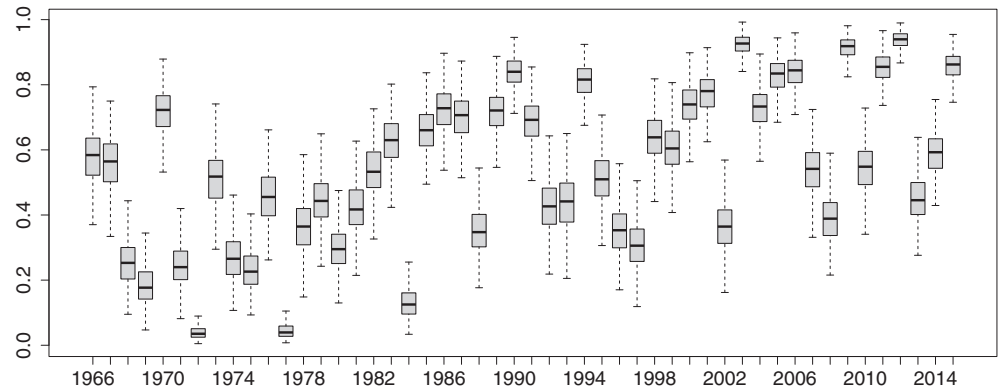


**FIGURE 6** Posterior probabilities of increments of average temperatures  $\{\bar{Y}_{D5}(\mathbf{s}) - \bar{Y}_{D1}(\mathbf{s}) > c\}$  for  $c = 0, 1$  and  $2^\circ\text{C}$  [Colour figure can be viewed at [wileyonlinelibrary.com](http://wileyonlinelibrary.com)]

**FIGURE 7** Boxplots of the distribution of the extent for events based on yearly average temperatures  $\{\bar{Y}_t(\mathbf{s}) - \tilde{\mu}(\mathbf{s}) > 0\}$ , versus year



It is noteworthy that the analysis of both probabilities and extents shows that consequences of global warming are stronger in average temperatures than in daily temperatures.

### 4.1.3 | Analysis of temperature increments between decades

This section summarizes the analysis of events that quantify the global warming in terms of the increments of

average temperatures,  $\{\bar{Y}_{D5}(\mathbf{s}) - \bar{Y}_{D1}(\mathbf{s}) > c\}$  for values  $c = 0, 1$  and  $2^\circ\text{C}$ .

#### Surface of probabilities

According to Figure 9 the risk of a positive increment of average temperatures between  $D1$  and  $D5$  is virtually 1 all over the region, except in the NW where it takes values around 0.7. However, for other  $c$  values, the spatial variability is higher. The risk of an increment higher than  $1^\circ\text{C}$ , is close to 1 in some areas and higher than 0.6 except in the NW where it is roughly 0.25. The risk of

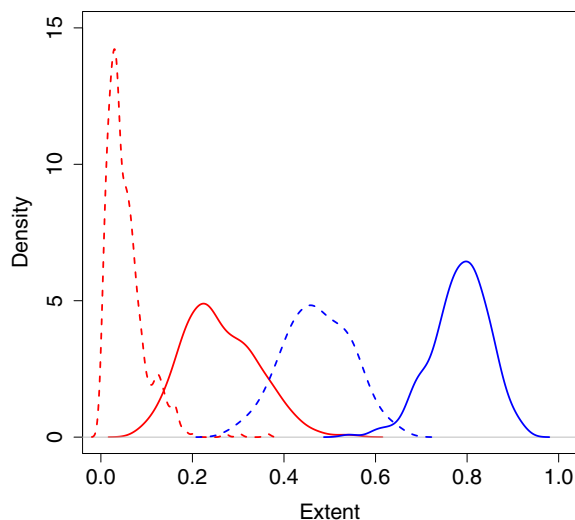


**FIGURE 8** Posterior mean across years of the yearly average extents for events  $\{Y_{t,\ell}(\mathbf{s}) - \tilde{\mu}(\mathbf{s}) > 0\}$  for  $\mathcal{B} = \mathcal{D}$  (black),  $\mathcal{V}$  (blue) and  $\mathcal{P}$  (red), and corresponding regression lines [Colour figure can be viewed at [wileyonlinelibrary.com](http://wileyonlinelibrary.com)]

**TABLE 3** Posterior mean and CI of the extent for events  $\{\bar{Y}_{D5}(\mathbf{s}) - \bar{Y}_{D1}(\mathbf{s}) > c\}$  for different values  $c$

| $c$           | $0^\circ\text{C}$ | $1^\circ\text{C}$ | $2^\circ\text{C}$ |
|---------------|-------------------|-------------------|-------------------|
| $\mathcal{D}$ | 0.95 (0.90, 0.98) | 0.69 (0.58, 0.80) | 0.25 (0.15, 0.36) |
| $\mathcal{V}$ | 0.98 (0.95, 1.00) | 0.80 (0.68, 0.89) | 0.32 (0.18, 0.47) |
| $\mathcal{P}$ | 0.93 (0.85, 0.98) | 0.63 (0.45, 0.79) | 0.19 (0.07, 0.36) |

Note: Shown for the entire region (first row) and for the valley and Pyrenees regions (second and third rows).

increments higher than  $2^\circ\text{C}$  is lower than 0.4 in most of the region except some small areas in the centre of the valley and the NE, where it attains 0.7. Comparing these results with the analysis of daily increments in sect. S4.1 of Data S1, we note that the risk of an increment between  $D1$  and  $D5$  higher than  $c$  is much higher for average temperatures than for daily temperatures.

### Extents

The first row of Table 3 summarizes the means and the 90% CI of the extents for increments between average temperature in  $D1$  and  $D5$ . The CI of the extents show that between 90 and 98% of the area under study has suffered a positive increment of the average temperatures, from 58% to 80% an increment higher than  $1^\circ\text{C}$ , and from 15% to 36% higher than  $2^\circ\text{C}$ .

## 4.2 | Comparison of the evolution in areas with different climates

The region considered in this analysis includes areas with very different climates (see Figure 1). Here, we analyse

whether the consequences of global warming are the same over the entire region or whether we can identify different patterns of evolution over time. This type of study is not possible using the observed database, since the number of available stations in some areas is sparse. The use of the output from the statistical model enables that type of comparison. More precisely, in this section, we use the approach described in section 3 to compute the extent for different events in two regions with different climates, and to compare the effects of global warming in those areas.

We consider two important regions in the study area, which according to the Köppen's climate classification have very different characteristics. Region  $\mathcal{V}$  (valley) is the area between parallels  $41^\circ\text{N}$  and  $42^\circ\text{N}$  with the semi-arid Bsk climate. It covers the central Ebro valley and it has a mean elevation of 373 m. This area is the most populated in Aragón, and the most important farming areas in the region are located there. Region  $\mathcal{P}$  (Pyrenees) is a mountainous area in the Pyrenees, over parallel  $42^\circ\text{N}$ , with mountain climate Cfb and some small areas with high mountain climates Dfb and Dfc. The mean elevation is 1427 m but in some points the elevation is over 3000 m. The last glaciers in Spain are located in this area.

### 4.2.1 | Average extents for increments of daily maximum temperatures over $\tilde{\mu}(\mathbf{s})$

Table 4 summarizes the mean of the average extent in D-JJA for events  $\{Y_{t,\ell}(\mathbf{s}) - \tilde{\mu}(\mathbf{s}) > c\}$ , for  $c = 0$  and  $2^\circ\text{C}$  in decades  $D1$  and  $D5$  and regions  $\mathcal{V}$  and  $\mathcal{P}$ , and for the analogous events defined with  $k = 2$  and 3 consecutive days.

The increase in extent between decades  $D1$  and  $D5$  is observed in both regions, but it is clearly higher in  $\mathcal{V}$ . The mean of the average extent in  $D1$  is quite similar in both regions. However, clear differences appear in  $D5$ , especially for the mildest events with  $c = 0$ : the mean of the percentage of area with daily maximum temperatures higher than the reference mean is 60% in  $\mathcal{V}$  and 54% in  $\mathcal{P}$ . These differences become smaller in more exigent events; for example, the mean of the percentage of area with increments over  $\mu(\mathbf{s})$  higher than  $2^\circ\text{C}$  during three consecutive days is 24% in  $\mathcal{V}$  and 20% in  $\mathcal{P}$ . However, in both regions the increase is clear since the counterpart in  $D1$  is 13%.

Figure 5 shows the evolution over time of the mean of the average extent in JJA in 1 year for events  $\{Y_{t,\ell}(\mathbf{s}) - \tilde{\mu}(\mathbf{s}) > 0\}$  in  $\mathcal{V}$ ,  $\mathcal{P}$ , and in the entire region  $\mathcal{D}$  for the sake of comparison. The corresponding fitted linear regressions are also plotted. A roughly linear increase is observed in both regions, but with different trends, 0.0038 and 0.0026, respectively; that means an increase in extent per decade of 3.8 in  $\mathcal{V}$ , and 2.6% in  $\mathcal{P}$ .



**TABLE 4** Posterior mean of the average extent in D-JJA for increments of daily maximum temperature over the reference mean higher than  $c$  with different persistence for reference values  $c = 0$  and  $2^\circ\text{C}$ , in decades  $D1$  (1966–1975) and  $D5$  (2006–2015) and regions  $\mathcal{V}$  and  $\mathcal{P}$

| $c$                                                        | $0^\circ\text{C}$ |               |               |               | $2^\circ\text{C}$ |               |               |               |
|------------------------------------------------------------|-------------------|---------------|---------------|---------------|-------------------|---------------|---------------|---------------|
|                                                            | $D1$              |               | $D5$          |               | $D1$              |               | $D5$          |               |
| Decade                                                     | $\mathcal{V}$     | $\mathcal{P}$ | $\mathcal{V}$ | $\mathcal{P}$ | $\mathcal{V}$     | $\mathcal{P}$ | $\mathcal{V}$ | $\mathcal{P}$ |
| $\{Y_{t,\ell}(\mathbf{s}) - \tilde{\mu}(\mathbf{s}) > 0\}$ | 0.45              | 0.44          | 0.60          | 0.54          | 0.29              | 0.29          | 0.42          | 0.38          |
| $\{Y_{t,\ell}(\mathbf{s}) - \tilde{\mu}(\mathbf{s}) > 2\}$ | 0.34              | 0.33          | 0.49          | 0.43          | 0.19              | 0.19          | 0.31          | 0.27          |
| $\{Y_{t,\ell}(\mathbf{s}) - \tilde{\mu}(\mathbf{s}) > 3\}$ | 0.26              | 0.26          | 0.41          | 0.35          | 0.13              | 0.13          | 0.24          | 0.20          |
| $\{\bar{Y}_D(\mathbf{s}) - \tilde{\mu}(\mathbf{s}) > 0\}$  | 0.27              | 0.24          | 0.84          | 0.62          | 0.01              | 0.01          | 0.19          | 0.10          |

Note: The mean of the extent for increments of average temperatures are shown in the last row.

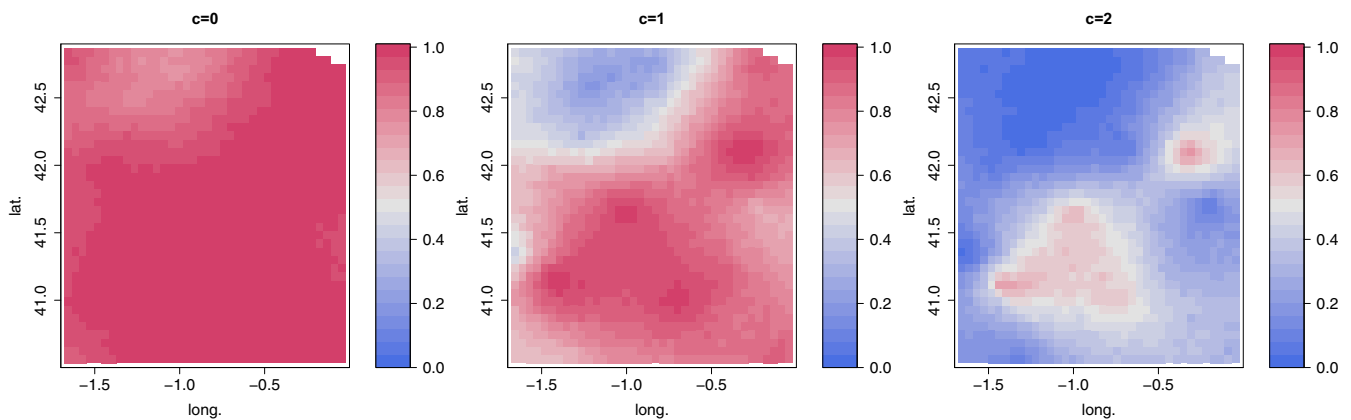


**FIGURE 9** Probabilities of events  $\{\bar{Y}_D(\mathbf{s}) - \tilde{\mu}(\mathbf{s}) > 0\}$  (first row), and  $\{\bar{Y}_D(\mathbf{s}) - \tilde{\mu}(\mathbf{s}) > 1\}$  (second row) in decades  $D1$  and  $D5$  and differences between them [Colour figure can be viewed at [wileyonlinelibrary.com](http://wileyonlinelibrary.com)]

#### 4.2.2 | Extents for increments of average temperatures over $\tilde{\mu}(\mathbf{s})$

The last row in Table 4 summarizes the mean of the extents for events  $\{\bar{Y}_D(\mathbf{s}) - \tilde{\mu}(\mathbf{s}) > c\}$  with  $c = 0$  and  $2^\circ\text{C}$ . In  $D1$ , the mean percentage of area with average temperature higher than the reference mean is quite similar in both regions, around 25%. However, relevant differences appear in  $D5$ , where the mean percentage is 84 in  $\mathcal{V}$  and 62% in  $\mathcal{P}$ . The posterior density of the extents, shown in Figure S4, enables us to quantify the uncertainty of the extent and it confirms the shift in location of the distribution of the extent in  $D5$  between the two regions. In  $D1$ , the posterior probability of the extent for a positive increment over  $\tilde{\mu}(\mathbf{s})$  in  $\mathcal{V}$  being higher than in  $\mathcal{P}$  is 0.57 and in  $D5$ , 0.94.

#### 4.2.3 | Extents for increments between average temperatures in $D1$ and $D5$

Finally, we compare the extent for increments of average temperature,  $\{\bar{Y}_{D5}(\mathbf{s}) - \bar{Y}_{D1}(\mathbf{s}) > c\}$  in  $\mathcal{V}$  and  $\mathcal{P}$ . Table 3 summarizes the mean of those extents for  $c = 0, 1$  and

$2^\circ\text{C}$ . The mean percentage of area with a positive increment is high in both regions, 98% and 93%, respectively. However, there are differences in the extent of more strict events; for example, the percentage of area with an increment higher than  $c = 1^\circ\text{C}$  is 80% in  $\mathcal{V}$  and 63% in  $\mathcal{P}$ . The posterior density of the extents, shown in Figure S4, allows us to quantify the uncertainty. The posterior probability of the extent for a positive increment in  $\mathcal{V}$  being higher than in  $\mathcal{P}$  is 0.96 and for increments higher than 1 and  $2^\circ\text{C}$ , 0.94 and 0.87, respectively.

To sum up, the increase in the extent of all the considered events is stronger in  $\mathcal{V}$  than in  $\mathcal{P}$ , although the magnitude of the increase depends on the type of event.

## 5 | CONCLUSIONS AND FUTURE WORK

Acknowledging that climate change with regard to temperature is occurring both temporally and spatially, we have presented an analysis to quantify this change at different time scales in a Mediterranean region around Aragón (NE of Spain), for 60 years from 1956 to 2015. The analysis is based on daily maximum temperature time

series from 18 locations, and a collection of spatially referenced time series of temperature data generated from a Bayesian model fitted to them. More precisely, to assess the changes on temperature in a space–time framework, we analyse exceedance events around the centre of the temperature distribution. We offer two basic ideas: (i) surfaces of probabilities which capture the spatial variation in the chance of an exceedance event and provide climate risk maps and (ii) extents which, for a subregion of interest, capture the expected proportion of incidence of a given exceedance event over the region. We define exceedance events in terms of a local mean value or increments between two decades, but other definitions of interest could be used. These quantities are defined at daily scale and can be averaged to any other temporal scale of interest.

Comparison of temperature evolution has been presented at daily and seasonal scale both temporally between decades and spatially between subregions. The analysis reveals that there is an increase all over the region in all the features and events used to quantify the evolution of temperature from 1966 to 2015. However, that increase is not spatially homogeneous, with the largest increase arising in the centre of the Ebro valley and NE area. The use of different events allows to quantify specific features, for example, the probability of a daily maximum temperature higher than the reference mean has increased roughly 0.2 from decade *D1* (1966–1975) to *D5* (2006–2015), attaining values higher than 0.7 in some areas. As expected, the increase in features based on average temperatures is stronger: the probability of the average temperature being higher than the reference mean has increased from *D1* to *D5* a value around 0.5, being virtually 1 in some areas. In all of the region except a small NW area, the risk of a positive increment in the average temperatures between *D1* and *D5* is virtually 1, and the risk of an increase higher than 1°C is higher than 0.5, and close to 1 in the south central part of the valley and NE.

Concerning the spatial incidence in the entire region, the extent of daily maximum temperature higher than the reference mean has increased 3.5% per decade. The mean of the extent with a positive average increment between *D1* and *D5* is 0.95. The suggested tools are also used to compare the evolution of the extent in different regions. We found that, in all the considered features, the increase in extent in region  $\mathcal{V}$ , with a semiarid climate, is higher than in  $\mathcal{P}$ , with a mountain climate. We showed that in *D1* the extent of the average temperature higher than the reference mean is roughly 0.25 in both regions while in *D5* it increases to 0.84 in  $\mathcal{V}$ , and 0.62 in  $\mathcal{P}$ . These results are consistent with those in Peña-Angulo et al. (2021) and Haug et al. (2020), who found a stronger

change in summer mean temperatures in the centre of the Ebro valley.

It is noteworthy that the suggested approach based on the analysis of collection of spatially referenced time series of temperature data has important advantages versus the analysis of usually spatially scarce observed data. Although some empirical measures, such as the extent, could be directly computed from an observed dataset, in many cases, they would be based on too few stations. Further, using only observed series, even spatially dense gridded series, uncertainty cannot be easily quantified, and probabilities or CIs such as those suggested in this work, cannot be computed.

The proposed ideas can be applied to any region of interest. All that is required is an adequate SWG or model able to generate replicates of temperatures series at a fine grid of geo-coded locations in that region. Future work will investigate other regions of interest, making further comparisons. We will also investigate events involving extremes of temperature, using suitable extreme value modelling, and compound events defined in terms of maximum and minimum temperatures or other climate variables. Further, we will explore other spatially referenced weather time series. We also will attempt to forecast future temperature change, using a suitable version of our modelling, applied to climate scenarios.

## AUTHOR CONTRIBUTIONS

**Ana C. Cebrián:** Conceptualization; methodology; formal analysis; writing – original draft; writing – review and editing. **Jesús Asín:** Conceptualization; methodology; formal analysis; writing – original draft; writing – review and editing. **Jorge Castillo-Mateo:** Conceptualization; methodology; formal analysis; writing – original draft; writing – review and editing. **Alan E. Gelfand:** Conceptualization; methodology; formal analysis; writing – original draft; writing – review and editing. **Jesús Abaurrea:** Conceptualization; methodology; formal analysis; writing – original draft; writing – review and editing.

## ACKNOWLEDGEMENTS

This work has been supported in part by the Grants PID2020-116873GB-I00 and TED2021-130702B-I00 funded by MCIN/AEI/10.13039/501100011033 and Unión Europea NextGenerationEU, and the Research Group E46\_20R: Modelos Estocásticos funded by Gobierno de Aragón. Jorge Castillo-Mateo was supported by the Doctoral Scholarship ORDEN CUS/581/2020 funded by Gobierno de Aragón. The authors thank AEMET for providing the data. The authors are grateful to the Editor and two Referees for their insightful and constructive remarks on an earlier version of the paper.

## CONFLICT OF INTEREST STATEMENT

The authors declare no conflicts of interest.

## DATA AVAILABILITY STATEMENT

Code in R and daily temperature series used to fit the model are available from the corresponding author upon reasonable request.

## ORCID

Ana C. Cebrián  <https://orcid.org/0000-0002-9052-9674>

Jesús Asín  <https://orcid.org/0000-0002-0174-789X>

Jorge Castillo-Mateo  <https://orcid.org/0000-0003-3859-0248>

Alan E. Gelfand  <https://orcid.org/0000-0002-5671-9212>

## REFERENCES

- Banerjee, S., Carlin, B.P. & Gelfand, A.E. (2014) *Hierarchical modeling and analysis for spatial data*, 2nd edition. New York, NY: Chapman and Hall/CRC.
- Bolin, D. & Lindgren, F. (2015) Excursion and contour uncertainty regions for latent Gaussian models. *Journal of the Royal Statistical Society: Series B (Statistical Methodology)*, 77, 85–106.
- Caraway, N.M., McCreight, J.L. & Rajagopalan, B. (2014) Multisite stochastic weather generation using cluster analysis and k-nearest neighbor time series resampling. *Journal of Hydrology*, 508, 197–213.
- Castillo-Mateo, J., Lafuente, M., Asín, J., Cebrián, A.C., Gelfand, A.E. & Abaurrea, J. (2022) Spatial modeling of day-within-year temperature time series: an examination of daily maximum temperatures in Aragón, Spain. *Journal of Agricultural, Biological and Environmental Statistics*, 27, 487–505.
- Cebrián, A.C., Asín, J., Gelfand, A.E., Schliep, E.M., Castillo-Mateo, J., Beamonte, M.A. et al. (2022) Spatio-temporal analysis of the extent of an extreme heat event. *Stochastic Environmental Research and Risk Assessment*, 36, 2737–2751.
- Chandler, R. & Scott, M. (2011) *Statistical methods for trend detection and analysis in the environmental sciences*. Hoboken, NJ: John Wiley & Sons.
- Chazarra-Bernabé, A., Flórez García, E., Peraza Sánchez, B., Tohá Rebull, T., Lorenzo Mariño, B., Criado, E. et al. (2018) *Mapas climáticos de España (1981–2010) y ETo (1996–2016)*. Agencia Estatal de Meteorología.
- Craigmile, P.F. & Guttorp, P. (2011) Space-time modelling of trends in temperature series. *Journal of Time Series Analysis*, 32, 378–395.
- Crimp, S., Bakar, K.S., Kokic, P., Jin, H., Nicholls, N. & Howden, M. (2015) Bayesian space-time model to analyse frost risk for agriculture in southeast Australia. *International Journal of Climatology*, 35, 2092–2108.
- Dowlatabadi, H. & Morgan, M.G. (1993) Integrated assessment of climate change. *Science*, 259, 1813–1932.
- French, J.P. (2017) Autoimage: multiple heat maps for projected coordinates. *R Journal*, 9, 284–297.
- García-Valero, J.A., Montávez, J.P., Gómez-Navarro, J. & Jiménez-Guerrero, P. (2015) Attributing trends in extremely hot days to changes in atmospheric dynamics. *Natural Hazards and Earth System Sciences*, 15, 2143–2159.
- Gelfand, A.E. & Smith, A.F. (1990) Sampling-based approaches to calculating marginal densities. *Journal of the American Statistical Association*, 85, 398–409.
- Gil Alana, L.A. & Sauci, L. (2019) US temperatures: time trends and persistence. *International Journal of Climatology*, 39, 5091–5103.
- Hartmann, D., Klein Tank, A., Rusticucci, M., Alexander, L., Brönnimann, S., Charabi, Y. et al. (2013) In: Stocker, T., Qin, D., Plattner, G.-K., Tignor, M., Allen, S., Boschung, J. et al. (Eds.) *Climate change 2013: the physical science basis. Contribution of working group I to the fifth assessment report of the Intergovernmental Panel on Climate Change*. Cambridge: Cambridge University Press.
- Haug, O., Thorarinsdottir, T.L., Sørbye, S.H. & Franzke, C.L. (2020) Spatial trend analysis of gridded temperature data at varying spatial scales. *Advances in Statistical Climatology, Meteorology and Oceanography*, 6, 1–12.
- IPCC. (2018) Summary for policymakers. In: Masson-Delmotte, V., Zhai, P., Pörtner, H.-O., Roberts, D., Skea, J., Shukla, P.R. et al. (Eds.) *Global warming of 1.5°C. An IPCC special report on the impacts of global warming of 1.5°C above pre-industrial levels and related global greenhouse gas emission pathways, in the context of strengthening the global response to the threat of climate change, sustainable development, and efforts to eradicate poverty*. Geneva: World Meteorological Organization.
- Katz, R.W. (2002) Techniques for estimating uncertainty in climate change scenarios and impact studies. *Climate Research*, 20, 167–185.
- Keellings, D. & Moradkhani, H. (2020) Spatiotemporal evolution of heat wave severity and coverage across the United States. *Geophysical Research Letters*, 47, e2020GL087097.
- Khan, N., Shahid, S., Ismail, T., Ahmed, K. & Nawaz, N. (2019) Trends in heat wave related indices in Pakistan. *Stochastic Environmental Research and Risk Assessment*, 33, 287–302.
- Kleiber, W., Katz, R.W. & Rajagopalan, B. (2013) Daily minimum and maximum temperature simulation over complex terrain. *The Annals of Applied Statistics*, 7, 588–612.
- Li, J. & Thompson, D.W. (2021) Widespread changes in surface temperature persistence under climate change. *Nature*, 599, 425–430.
- Lyon, B., Barnston, A.G., Coffel, E. & Horton, R.M. (2019) Projected increase in the spatial extent of contiguous US summer heat waves and associated attributes. *Environmental Research Letters*, 14, 114029.
- Masson-Delmotte, V., Zhai, P., Pirani, A., Connors, S.L., Péan, C., Berger, S. et al. (2021) *Climate change 2021: the physical science basis. Contribution of working group I to the sixth assessment report of the Intergovernmental Panel on Climate Change*. Geneva: IPCC.
- Peña-Angulo, D., Gonzalez-Hidalgo, J.C., Sardonis, L., Beguería, S., Tomas-Burguera, M., López-Bustins, J.A. et al. (2021) Seasonal temperature trends on the Spanish mainland: a secular study (1916–2015). *International Journal of Climatology*, 41, 3071–3084.
- Pfleiderer, P. & Coumou, D. (2018) Quantification of temperature persistence over the Northern Hemisphere land-area. *Climate Dynamics*, 51, 627–637.
- Rebetez, M., Dupont, O. & Giroud, M. (2009) An analysis of the July 2006 heatwave extent in Europe compared to the record year of 2003. *Theoretical and Applied Climatology*, 95, 1–7.

- Schliep, E.M., Gelfand, A.E., Abaurrea, J., Asín, J., Beamonte, M.A. & Cebrián, A.C. (2021) Long-term spatial modelling for characteristics of extreme heat events. *Journal of the Royal Statistical Society: Series A (Statistics in Society)*, 184, 1070–1092.
- Smith, K., Strong, C. & Rassoul-Agha, F. (2018) Multisite generalization of the sharp weather generator. *Journal of Applied Meteorology and Climatology*, 57, 2113–2127.
- Sommerfeld, M., Sain, S. & Schwartzman, A. (2018) Confidence regions for spatial excursion sets from repeated random field observations, with an application to climate. *Journal of the American Statistical Association*, 113, 1327–1340.
- Tye, M.R., Katz, R.W. & Rajagopalan, B. (2019) Climate change or climate regimes? Examining multi-annual variations in the frequency of precipitation extremes over the Argentine pampas. *Climate Dynamics*, 53, 245–260.
- Verdin, A., Rajagopalan, B., Kleiber, W., Podestá, G. & Bert, F. (2019) BayGEN: a Bayesian space-time stochastic weather generator. *Water Resources Research*, 55, 2900–2915.
- Wilks, D.S. (1999) Simultaneous stochastic simulation of daily precipitation, temperature and solar radiation at multiple sites in complex terrain. *Agricultural and Forest Meteorology*, 96, 85–101.
- Wilks, D.S. (2009) A gridded multisite weather generator and synchronization to observed weather data. *Water Resources Research*, 45, W10419.
- Zscheischler, J., Martius, O., Westra, S., Bevacqua, E., Raymond, C., Horton, R.M. et al. (2020) A typology of compound weather and climate events. *Nature Reviews Earth & Environment*, 1, 333–347.
- Zwiers, F.W. & Von Storch, H. (1995) Taking serial correlation into account in tests of the mean. *Journal of Climate*, 8, 336–351.

## SUPPORTING INFORMATION

Additional supporting information can be found online in the Supporting Information section at the end of this article.

**How to cite this article:** Cebrián, A. C., Asín, J., Castillo-Mateo, J., Gelfand, A. E., & Abaurrea, J. (2023). Assessing space and time changes in daily maximum temperature in the Ebro basin (Spain) using model-based statistical tools. *International Journal of Climatology*, 1–16. <https://doi.org/10.1002/joc.8305>